In situ precipitation of Nickel–hexacyanoferrate within multi-walled carbon nanotube modified electrode and its selective hydrazine electrocatalysis in physiological pH

Article *in* Journal of Electroanalytical Chemistry · May 2011

DOI: 10.1016/j.jelechem.2011.01.022

CITATIONS
43

READS
311

3 authors:

Annamalai Senthil Kumar
VIT University
228 PUBLICATIONS **4,567** CITATIONS
SEE PROFILE

Barathi Palani
Pondicherry University
17 PUBLICATIONS **356** CITATIONS
SEE PROFILE

Karnam Chandrasekara Pillai
University of Madras
82 PUBLICATIONS **1,507** CITATIONS
SEE PROFILE

Journal of Electroanalytical Chemistry 654 (2011) 85–95

Contents lists available at ScienceDirect

Journal of Electroanalytical Chemistry

journal homepage: www.elsevier.com/locate/jelechem

In situ precipitation of Nickel-hexacyanoferrate within multi-walled carbon nanotube modified electrode and its selective hydrazine electrocatalysis in physiological pH

Annamalai Senthil Kumar [a,*], Palani Barathi [a], K. Chandrasekara Pillai [b]

[a] Environmental and Analytical Chemistry Division, School of Advanced Sciences, Vellore Institute of Technology University, Vellore 632 014, India
[b] Department of Chemical Engineering, National Taiwan University of Science and Technology, Taipei 106, Taiwan

ARTICLE INFO

Article history:
Received 30 August 2010
Received in revised form 11 January 2011
Accepted 17 January 2011
Available online 26 January 2011

Keywords:
Carbon nanotube
Nickel-hexacyanoferrate
In-situ preparation
Electrocatalysis
Hydrazine

ABSTRACT

Hybrid nickel-hexacyanoferrate-functionalized multiwalled carbon nanotube modified glassy carbon electrode (GCE/Ni-NCFe@f-MWCNT) has been prepared using electrodeposited Ni on functionalized MWCNT modified GCE (GCE/Ni@f-MWCNT) as a template and $[Fe(CN)_6]^{3-}$ as an *in-situ* chemical precipitant, without any additional linker. Characterization of the GCE/Ni-NCFe@f-MWCNT by X-ray diffraction, X-ray photoelectron spectroscopy, field emission scanning electron microscopy, energy dispersive X-ray analysis, transmission electron microscopy and cyclic voltammetry (CV) collectively revealed that the functionalized MWCNT is effective to uptake large amount of Ni species and, in turn, substantial quantity of Ni-NCFe units within its internal structure. Cyclic voltammetry of the GCE/Ni-NCFe@f-MWCNT showed non-stoichiometric K^+/e^- and insertion/exertion behavior ($\partial E_{pa}/\partial \log [KCl] = 42.9$ and ($\partial E_{pc}/\partial \log [KCl] =$ 117 mV/decade) due to some kinetic limitation to the insertion of K^+ ion through the hydrophobic basal planes of the hybrid electrode. A quantitative model has been proposed to estimate the influencing components (underlying support, surface functional groups, basel plane, impurities, and insertion into edge-plane defects) in the formation of the hybrid Ni@f-MWCNT and, in turn, the Ni-NCFe@f-MWCNT. Electrocatalytic hydrazine oxidation on the GCE/Ni-NCFe@f-MWCNT showed 33 times enhancement in the current signal over GCE/f-MWNT in a pH 7 phosphate buffer solution. Amperometric *i–t* method of hydrazine detection yielded current sensitivity and calibration range of 120.2 μA/μM and 20–200 μM, respectively. The hybrid GCE/Ni-NCFe@f-MWCNT material is tolerable to other co-existing interferences such as oxalic acid, citric acid and nitrite. Finally, three different water real sample analyses were successfully demonstrated with appreciable recovery values.

1. Introduction

Hybrid carbon nanotube-inorganic/organic molecular moieties possessing new class of functional materials with synergistic effect of the individuals have gained tremendous interest in recent timings owing to their exceptional physical and chemical properties including stabilizing of unusual intermediate species of chemical, biochemical and biomedical interest with enhanced performance towards applications [1–3]. Nickel-hexacyanoferrate (Ni-NCFe) is a mixed-valent inorganic polymer analogue from Prussian blue (PB) family [4], having zeolite type of macro-molecular crystal structures [4,5], useful for various technological applications [6–8], including electro-chemical and -biochemical sensing of small molecules viz., hydrazine [9,10], hydrogen peroxide [11,12], dopamine [13,14], nitric oxide [15] and reduced nicotinamide adenine dinucleotide (NADH) [16,17], which in turn led to *dehydrogenase* enzyme-coupled biosensors [18]. Ni-NCFe and other PB analogues have strong alkali metal-ion dependent property and the naked compounds disintegrate at pH > 4 [6–8,19–22]. For unknown reasons, the alkali metal-ions (Na^+ or K^+) in the buffer solution are not found to be solely useful to maintain the electrical neutrality of the naked materials [6–8,19–22]. In order to solve the problem, extra Na^+- and K^+-containing electrolyte was added as free ions to the working buffer solution [9,11,16,23]. Meanwhile, nafion, a perfluoro-cation exchange polymer, over layer-coated and sol–gel composed matrixes were reported as dressed Ni-NCFe materials to arrest the disintegration steps, and hence, leading to neutral buffer solution-based electrochemical applications [9,10,14]. However, such processes can considerably reduce the out put current signals and increase the internal resistance of the systems. Interestingly, here in we report a hybrid Ni-NCFe/functionalized multi-walled carbon nanotube modified glassy carbon electrode (designated as GCE/Ni-NCFe@f-MWCNT, GCE = glassy

* Corresponding author. Tel.: +91 416 2202754.
E-mail address: askumarchem@yahoo.com (A. Senthil Kumar).

1572-6657/$ - see front matter © 2011 Elsevier B.V. All rights reserved.
doi:10.1016/j.jelechem.2011.01.022

carbon electrode and f = functionalized), prepared by cathodically deposited Ni on f-MWCNT modified GCE as a template (GCE/Ni@f-MWCNT) and $[Fe(CN)_6]^{3-}$ as a precipitant, as a stable material for physiological solution (pH 7 sodium phosphate buffer solution, PBS) and for enhanced electrochemical and electrocatalytic applications.

Conventionally, bulk Ni-metal was used as a source to form thin film of Ni-NCFe using millimolar solution of $[Fe(CN)_6]^{3-}$ dissolved in ~0.1 M alkali metal ion, preferably with Na^+ ions, either by immersion or by potentiostatic polarization methods [21,22]. Since the approach uses the reaction associated with corrosion mechanism (Ni^{2+} ion formation) to form a new interface, it may plug-off certain portions of the underlying metal along with the Ni-NCFe flaking into the solution. Because of these problems this preparation approach was less commonly used for application purpose in the literature [16]. On the other hand, no such complications were reported in several other extended methods in which fine and nano Ni^0, Ni^{2+} or $[Fe(CN)_6]^{3-}$ species were incorporated into matrixes, such as, 3,3-thiodipropionic acid self assembled-Au [23], starbust poly(amidoamine) (PAMAM) dendrimer combined 3-mercaptopropionic acid or 2-aminoethanethiol self assembled Au [24], DNA [25], diamine functionalized paraffin wax chemically immobilized graphite electrodes [13] and carbon ceramic material [10]. However, electrochemical operation solely with neutral buffer solution could be rarely achieved [10].

Recently, few papers reported carbon nanotube (CNT) as matrix to prepare hybrid Ni-NCFe modified electrodes for selective electro-analytical applications, for example, CNT-Polyaniline-Ni-NCFe electrode for electrically switched ion-exchange [26,12], CNT-Ni-NCFe for glucose and cholesterol biosensor [11]. Note that those reported procedures adopted *ex-situ* preparation approach, in which, nanoparticles of Ni-NCFe were prepared discreetly by solution phase and/or electrochemical co-deposition procedure, in which a mixture containing $\{Ni^{2+} + [Fe(CN)_6]^{3-}_{soln}\}$ was first converted to nano Ni-NCFe particles, $\{Ni\text{-}NCFe\}_{nano}$, and then they were allowed to assemble/adsorb on the CNT ($CNT_{surface}\{Ni\text{-}NCFe\}_{nano}$) utilizing the effect of preloaded linker, such as, polyaniline, chitosan and histidine within the matrix [26,12]. However, good stability could not be achieved with these systems in pH 7 PBS without any free added alkaline metal ions. Meanwhile, *ex-situ* technique based hybrid CNT-Cobalt hexacyanoferrate (Co-NCFe@CNT) [27,28] and CNT-Cerium hexacyanoferrate (Ce-NCFe@CNT) [29] complexes were recently prepared and operated in pH 7 PBS [27]. First time in this work, we demonstrate a new *in-situ* preparation method for novel Ni-NCFe@f-MWCNT hybrid material formation on GCE, through sequential surface modification procedure with GCE/Ni@f-MWCNT and $[Fe(CN)_6]^{3-}$, which is also highly amenable for stable electrochemical and electrocatalytic application in pH 7 sodium PBS.

Hydrazine is an important chemical of environmental, industrial and pharmaceutical interest, and reported to be neurotoxin producing carcinogenic and mutagenic effects [30,31]. Sensitive and selective detection of the compound is of vital importance to address key issues about the hydrazine effect in the respective application settings. Another important reason for choosing hydrazine oxidation as a model reaction here was the following: N_2 and $4H^+$ being the reaction products of hydrazine oxidation, when they are produced within the interphase, more specially at the inter-walls of the Ni-NCFe@f-MWCNT, they may alter the local pH and disturb the internal structure and in turn may influence the stability of the hybrid network [19]. The present investigation with the hybrid Ni-NCFe@f-MWCNT material not only provides an elegant route to synthesize physiologically stable PB analogue, but also to understand the structural and electron-transfer features of the new hybrid CNT-macro-molecular inorganic units, which are least reported in the literature.

2. Experimental section

2.1. Reagents and materials

Mullti-walled carbon nanotube (>90% purity) and single-walled carbon nanotube (~70% purity) were purchased from Aldrich, USA. Nickel chloride hexahydrate ($NiCl_2.6H_2O$) was from Central drug house (P) Ltd, potassium ferricyanide from Merck specialties private Ltd and hydrazine sulphate extrapure from Sisco Research laboratories, India. Other chemicals were of analytical grade, and used as received without further purification. Aqueous solutions were prepared using deionized and alkaline $KMnO_4$ distilled water (designated as DD water). Unless otherwise stated, pH 7 PBS of ionic strength 0.1 M was used as supporting electrolyte in this study.

2.2. Apparatus

Voltammetric measurements were carried out using CHI model 660C electro-chemical work station, USA with 10 mL working volume. The three electrode system consisted of glassy carbon electrode (GCE) of 0.0707 cm^2 geometrical surface area and its chemically modified form (CME) as a working electrode, Ag/AgCl with 3 M KCl as a reference electrode and platinum wire as a counter electrode. The Bio-analytical system (BAS, USA) polishing kit was used to polish the GCE surface. The surface of the GCE was cleaned both mechanically and electrochemically by polishing with 1 μm alumina powder, washing with DD water and sonicating for 5 min followed by performing cyclic voltammetry (CV) for 10 cycles in the potential window 0 V to 0.9 V vs. Ag/AgCl at a potential scan rate (v) of 50 mV s^{-1} in pH 7 PBS.

2.3. Procedures

Functionalized MWCNT (i.e., f-MWCNT) was prepared by Tam's method in which a mixture of 200 mg of MWCNTs + 35 mL of 15 M HNO_3 was refluxed for 12 h in a silicone oil bath at 140 °C, filtered, washed with copious amount of DD H_2O until the pH of the filterant solution was neutral, and finally dried at 80 °C in a vacuum oven [32]. X-ray photoelectron spectroscopy (Ulvac-PHI, PHI500, Versaprobe) of the dried f-MWCNT material showed no detectable Fe impurity. In an another method, metal impurities within the MWCNT were removed without activating the carbon nanotube, as per the procedure suggested by Compton and workers, in which the commercial MWCNTs were stirred with 2 M dilute nitric acid for 35 h at room temperature and washed thoroughly with DD water (referred as p-MWCNT) [33]. For electrochemical analysis, 1 mg of the f-MWCNT was dispersed in 500 μL ethanol, as a stock solution. Prior to the surface coating, the stock was sonicated for 3–5 min and 3 μL of the suspension was drop-coated on the pre-treated GCE (designated as GCE/f-MWCNT), and allowed for 10 min for complete air-dry. The modified electrode was pre-treated in pH 7 PBS in the potential range 0 V to 0.9 V vs. Ag/AgCl at v = 50 mV s^{-1} for twenty continuous cycles (n = 20). There is no sign of any faradic electron-transfer behavior with this system. All experiments were performed with normal dissolved oxygen (DO), that is, closely resembling physiological systems.

Scheme 1 provides the new preparation procedure for the template-based GCE/Ni-NCFe@f-MWCNT material. The step-1 concerns with the preparation of GCE/Ni@f-MWCNT in which Ni metal was cathodically deposited on the GCE/f-MWCNT from a solution mixture containing 3 mM $NiCl_2$ dissolved in 0.1 M pH 7 PBS at an applied potential of -0.9 V vs. Ag/AgCl for 180 s (optimal). The above GCE/Ni@f-MWCNT electrode was used as a template in step-2 and immersed in 1 mM $K_3[Fe(CN)_6]$ containing 0.1 M PBS for 10 min. It was then washed with DD water and potential cycled

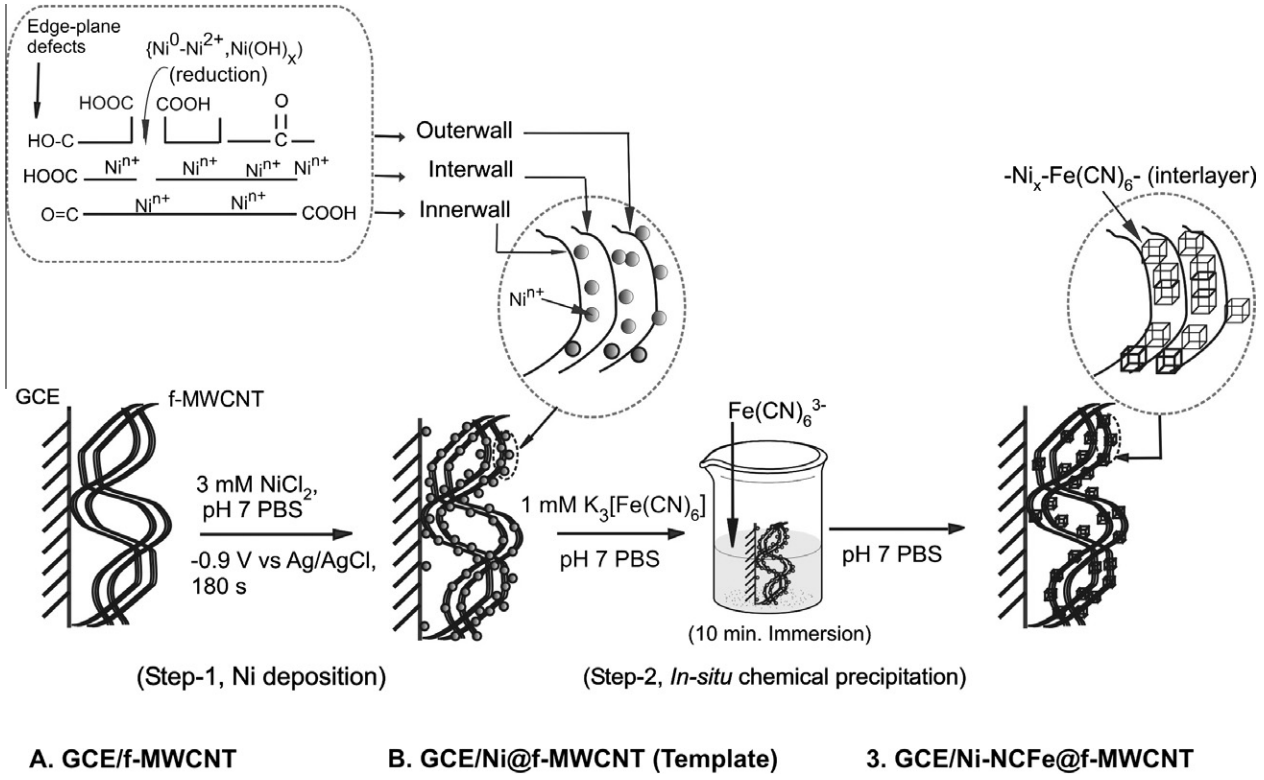

Scheme 1. Illustration for cathodically electrodeposited Ni on functionalized multiwalled carbon nanotube modified electrode for *in situ* precipitation of hybrid nickel-hexacyanoferrate particulate system.

in the range 0 V to 0.9 V for 20 times in pH 7 PBS at $v = 50$ mV s^{-1}. Note that the ionic radii of Ni^{2+} (0.83 Å) and $[Fe(CN)_6]^{3-}$ (2.9 Å) are [34] comparatively smaller in size than the nanotube diameter (100 Å), and hence these species can easily penetrate inside the CNT through the open ends and edge-plane defects. Surface active concentration of Ni-NCFe within f-MWCNT was calculated from the relation, $\Gamma_{\text{Ni-NCFe}} = Q_{pa}/nFA$, where Q_{pa} is the anodic peak area for the combined peaks, A1 and A2 (*vide infra*).

Due to practical difficulty, samples for X-ray diffraction (XRD) were prepared by simulated solution phase condition. First, for the case of Ni@f-MWCNT template sample, 10 mg of f-MWCNT was stirred with 30 mg of Ni^{2+} (12.6 mM) containing aqueous solution for about 2 h, filtered, washed with copious amount of water and dried in a desiccator. Next, for the case of Ni-NCFe@f-MWCNT sample, the above Ni@f-MWCNT template sample was immersed in $[Fe(CN)_6]^{3-}$ (14 mg, 4.2 mM) solution for 2 h, washed, filtered and stored in a desiccator until XRD measurements. In order to verify that the solution phase simulated Ni-NCFe@f-MWCNT sample and the *in-situ* prepared Ni-NCFe@f-MWCNT sample were the same chemically, it was confirmed by CV. The simulated powder samples were drop-coated on GCE, as described above, and its response, as illustrated in Fig. S1, showed well defined redox peaks with an $E^{o'}$ value of 325 mV vs. Ag/AgCl, comparable with the *in-situ* prepared Ni-NCFe@MWCNT redox response at 335 V vs. Ag/AgCl (*vide infra*), showing strong resemblance between the Ni-NCFe@MWCNT samples prepared by two different methods. Meanwhile, for the XRD authentication of the presence of Ni-NCFe units in the Ni-NCFe@MWCNT samples, naked Ni-NCFe powder sample was prepared by drop wise addition of 0.25 g of $NiCl_2$ (30 mM) dissolved in 35 mL water to 0.12 g of $K_3[Fe(CN)_6]$ (10 mM) dissolved in 35 mL of 0.026 g KCl (10 mM) solution under strong stirring for over-night at room temperature. Brown colored precipitate was separated out from the reaction mixture by centrifugation, washed with copious amount of water and dried in a desiccator for over-night. For the case of Transmission electron microscopy (TEM) analyses (TEM, JEOL-3010) of Ni-NCFe@f-MWCNT, the electrochemical procedure was adopted on Indium Tin Oxide (ITO) support, and then the film was dried and carefully pealed-off with doctor needle for measurements. For the Field emission scanning microscopy (FESEM, JEOL JSM-6700F), energy-dispersive X-ray analyses (EDXA) and X-ray photoelectron spectroscopy (XPS) analyses, screen-printed carbon electrodes modified with electrochemically prepared Ni@f-MWCNT and Ni-NCFe@f-MWCNT were used. In the XPS analyses C 1s peak at a binding energy (BE) = 284.6 eV was taken as internal reference. XPSPEAK41 software program was used for the deconvolution of the XPS peaks.

3. Results and discussion

3.1. Physicochemical characterization

Powder XRD responses of the f-MWCNT, Ni@f-MWCNT, Ni-NCFe and Ni-NCFe@f-MWCNT showed appreciable peaks indicating the presence of crystalline hybrid nano-materials within the respective matrixes (Fig. 1). For the case of f-MWCNT, apart from the standard 2θ peaks (26 and 42.7°) a peak at low angle, 11.8°, was discreetly noticed (Fig. 1A). The low angle peak is analogous to a recent report by Hae et al. for the hydroxyl, epoxide, and carboxyl functionalized graphite oxide (GO) surface at 12.84°(0 0 1) [35], which gives a first hand information for oxygen functional groups on the f-MWCNT. Recently, Compton and his co-workers pointed-out generation of large numbers of edge-plane like open-ended hole defects heavily decorated with oxygen functional groups (electro-active) on the f-MWCNT, similar to the GO, upon the acid-based functionalization procedure [36]. Meanwhile, our group recently reported a bulged nano-wall structure of the catechol encapsulated native-MWCNT material with an XRD peak at

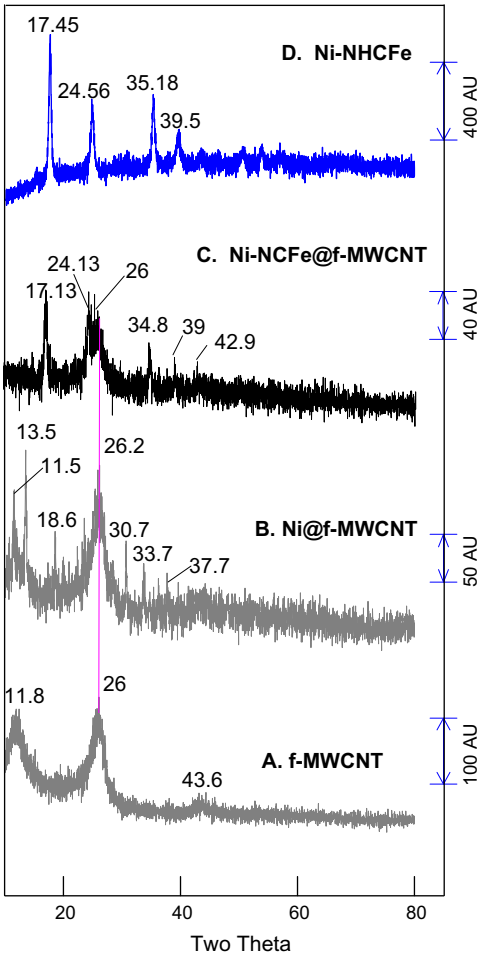

Fig. 1. XRD responses of f-MWCNT (A), Ni@f-MWCNT (B), Ni-NCFe@f-MWCNT (C), and naked Ni-NCFe (D).

a low angle, 11.28° [2]. Since there was no specific compound encapsulated in the present case, the principal factor responsible for the 11.8° peak (Fig. 1A) was the edge-plan defects and disordered wall structures only. On the other hand, the Ni@f-MWCNT yielded different 2θ peaks both at lower (11.5, 13.5 and 18.6°) and higher (30.7, 33.7 and 37.7°) angles with respect to the 26.2° peak of the MWCNT (Fig. 1B). Azadi et al. observed a higher angel 2θ peak at 37° for Ni particle bounded on the surface of the f-MWCNT (Ni@f-MWCNT) prepared by a solution phase wet method [37]. It may be noted that there is no precise matching model system available in literature to compare the lower angle peaks of the Ni@f-MWCNT material. However, from the recent report for the functionalized carbon nanotube-Fe-organometallic composite material with XRD peaks at 2θ values 11.8, 17.6, 20, 26.4, 28.6, 35.2, 39.3, 46.5 and 55.9° [37], it could be concluded that the metallic film or species might have deposited both on the outer and inner walls of the f-MWCNT. Since the f-MWCNT has numerous edge-plane defects, the electrochemical route for Ni deposition could have allowed the Ni^{2+} insertion into the defects and subsequent electrodeposition as metallic or oxyhydroxy Ni species inside the basal planes. Meanwhile, because of the metal ion-carbonyl/carboxyl group binding (chelating) tendency [38], the oxygen functional groups on f-MWCNT surface, presumably retained the Ni as charged species as Ni^{2+}. The XPS characterization results in the next section lend support to these propositions. Fig. 1C illustrates typical XRD pattern of the Ni-NCFe@f-MWCNT showing four predominant 2θ peaks at 17.13, 24.13, 34.8 and 39°, which are in good agreement with the cathodically deposited bulk Ni-NCFe values in the range 17–39° [4], and also with the authentic crystalline naked Ni-NCFe powder sample prepared in this work (Fig. 1D). Note that there is no peak observed at 2θ ~65° for the Ni-NCFe@f-MWCNT sample (Fig. 1C) indicating the absence of any soluble form of the Ni-NCFe [4] within its matrix.

The high-resolution XPS spectra of the Ni $2p_{3/2}$ core energy level for the Ni@f-MWCNT sample is shown in Fig. 2A. The Ni $2p_{3/2}$ energy level was centered around 856 eV with asymmetry in the higher binding energy side. The Ni $2p_{3/2}$ spectrum was deconvoluted for five differently bound Ni species with the BE values 854.4, 855.4, 856.4, 857.6 and 858.2 eV. The BE and full width at half maximum (FWHM) values and the corresponding possible species are listed in Table 1. Based on the literature on the XPS of the Ni metal and its oxy/hydroxides [39,40], passivated Cu-Ni alloy [41] and Ni adsorbed sodium decylbenzene-MWCNTs [42], the possible Ni species formed during the electrochemical reduction of $NiCl_2$ in pH 7 PBS in the present case could be identified as NiO (854.5 eV) [39,40], $Ni^{II}(OH)_x(H_2O)_y^{n+}$ (~855.4 eV) [41], Ni(II)-oxygen containing surface functional group complexes, such as, >C═O—Ni(II) and —COO—Ni(II) (856.1–856.5 eV) [40–42], $Ni^{II}(OH)_xCl_y^{n+}$ (~857.6) [40], and β-Ni^{III}OOH (858.1–861 eV) [39–41]. The high-valent β-Ni^{III}OOH species could be originated from chemical reaction between Ni species with H_2O_2, which might be generated as a intermediate species during the electrochemical reduction step in presence of dissolved oxygen in the PBS. Interestingly, there was no signal at 852.6 eV (data not included) corresponding to the metallic Ni^0 [40], suggesting the absence of any Ni^0 within the film and interface. It is expected that the >C═O—Ni(II) and its related Ni-complexes might exist in the surface edge-plane defects of the f-MWCNT, while the other Ni species including β-Ni^{III}OOH preferably situated in the inner CNT walls as buried sites as in Scheme 1. Fraction of insoluble NiO (854.4 eV) also formed during the cathodic deposition process, preferentially on the surface of the screen-printed carbon electrode/f-MWCNT. It is interesting to note that there was no detectable Fe $2p_{3/2}$ signal with the Ni@f-MWCNT sample (Fig. 2B) signifying negligible amount of the Fe impurity within the matrix.

The Ni $2p_{3/2}$ XPS pattern for the Ni-NCFe@f-MWCNT sample showed BE levels at 856.4 and 857.8 eV on deconvolution corresponding to the existence of N-terminal attached species of Ni with two different oxidation states, **Ni^{II}**-NC-Fe and **Ni^{III}**-**N**C-Fe-, respectively, in accordance with the BE values 856.5 and 858.4 eV reported for the same metal ion derived from bulk ruthenium oxide stabilized Ni-NCFe [43]. Further to this, the BE signals for Fe $2p_{3/2}$ at 708.6 eV (Fig. 2B) and N 1s at 398.1 eV (Fig. 2C) also matched well with the quoted values 708.4 and 398 eV [43,44], corresponding to iron as Ni-NC-**Fe^{III}** and nitrogen as $Ni^{III/II}$-**N**C-Fe^{III} sites. Also, the Ni $2p_{3/2}$ at a BE 854.5 eV with Ni-NCFe@f-MWCNT indicated that the insoluble NiO was still retained on the surface interface.

SEM pictures of f-MWNT, Ni@f-MWCNT and Ni-NCFe@MWCNT placed in Fig. 3A–F indicate fine coil-like nano structures on the electrode surface. There was no sign of any continuous metallic layer or film on the surfaces of the Ni and Ni-NCFe modified electrodes, supporting the XPS results (absence of metallic Ni^0). White spots of size ~20 nm on the top of the walls for both the Ni@f-MWCNT and Ni-NCFe@f-MWCNT samples confirmed the retaining of the insoluble NiO particles identified by XPS in the previous section. Meanwhile, fewer tinny white spots of smaller in size ~5 nm were noticed on the f-MWNT surface, which might be due to unknown impurities. EDXA results showed major elements with atomic% values for Ni-NCFe@f-MWCNT (for Ni@f-MWCNT) as follows (Fig. S2 and Table S1): Fe = 0.52 (0.02), Ni = 0.61 (0.56), N = 0.68 (0.0), Na = 0.61 (0.48), Cl = 6.06 (1.92) and K = 0.01 (0.04). It is somewhat unexpected that marked Na and Cl were

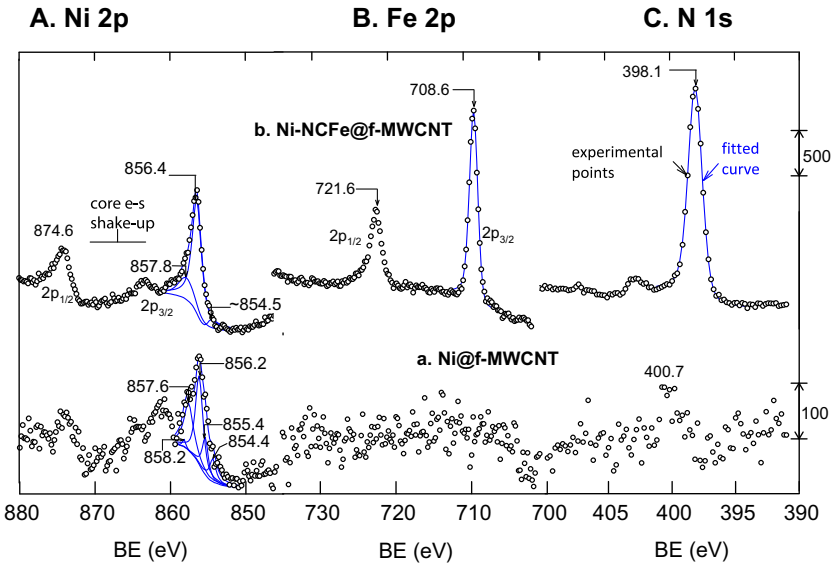

Fig. 2. XPS patterns for core energy level of Ni 2p (A), Fe 2p (B) and N 1s (C) for Ni@f-MWCNT (a) and Ni-NCFe@f-MWCNT (b) modified screen-printed carbon electrodes.

Table 1
XPS data for the Ni@f-MWNT and Ni-NCFe@f-MWNT modified screen-printed carbon electrodes.

Modified electrode	Element	Species[a]	BE (eV) (FWHM)
Ni@f-MWCNT	Ni $2p_{3/2}$	**Ni^{II}**—O=C<	856.2 (1.2)
		Ni^{II}$(OH)_x(Cl_y^{n+}$	857.6 (1.5)
		β-**Ni^{III}**OOH	858.2 (0.5)
		Ni^{II}$(OH)_x(H_2O)_y^{n+}$	855.4 (0.95)
		NiO	854.4 (1.0)
Ni-NCFe@f-MWCNT	Ni $2p_{3/2}$	**Ni^{III}**-NC-Fe	857.8 (1.0)
		Ni^{II}-NC-Fe	856.4 (1.1)
		NiO	854.5 (1.0)
	Fe $2p_{3/2}$	Ni-NC-**Fe^{III}**	708.6 (1.3)
	N 1s	Ni-**N**C-Fe	398.1 (1.3)

[a] Bold characters correspond to the denoting species. FWHM = full width at half maximum.

present within the Ni@f-MWCNT matrix. Since it has been reported that the MWCNT contains some frozen-water channels inside the capillary and walls [45,46], fractions of Na^+ ions from the PBS and Cl^- from the $NiCl_2$ might have penetrated into the interlayer and stabilized within the CNT. Ion-size effect might be involved in the selective intake of Na^+ and Cl^- rather than P from PO_4^{2-} (trace content identified, 0.22%). The atom% ratio between different elements for Ni-NCFe within the Ni-NCFe@f-MWCNT material were: Ni/Fe = 1.22, Ni/N = 0.89 and Ni/Na = 1, where as, in contrast, the bulk Ni-NCFe electrode showed "1" for all the ratios [44]. This difference in the internal atomic ratio of the Ni-NCFe@f-MWCNT is expected to cause specific changes in the physical properties including stability, electrochemical and electrocatalytic activities as shown below.

In order to precisely find out the exact position of the Ni-NCFe within the f-MWCNT, TEM was finally carried out (Fig. 4). It is interesting to notice tiny and well-structured rectangular nano spots (less clear at high magnification) along with marked enhancement in the tube diameter, 2.6 times higher over the unmodified carbon, suggesting that the macro-molecular Ni-NCFe might occupy the internal structure of the MWCNT as fine rectangular chains along the inter-walls of the carbon nanotube. Note that this feature is distinctly different from that observed in the case of the conventional *ex-situ* preparation of the Ni-NCFe@MWCNT with nano-spots out side the CNT walls [11]. The new observation in this work with the Ni-NCFe@f-MWCNT is unique in the hybrid macromolecule-CNT literature. The open-ended walls of the f-MWCNT could be seen in Fig. 4 as faded end due to the oxygen-rich surface functionalities of the edge-defects.

Concerning the Ni-NCFe@f-MWCNT formation mechanism, it is proposed that when the Ni@f-MWCNT template was immersed in $[Fe(CN)_6]^{3-}$/pH 7 PBS, the Ni species except NiO, could chemically precipitate as macro-molecular Ni-NCFe units and get stabilized as continuous chains within f-MWCNT. It is expected that the "Ni^{2+}-oxygen functional group" species also involved in the precipitation on the surface. Further CV characterization provided detailed interface structure of the new *in-situ* prepared Ni-NCFe@f-MWCNT electrode material.

3.2. Electrochemical characterization

Fig. 5A shows typical CV response of GCE/Ni-NCFe@f-MWCNT material prepared at optimal conditions in pH 7 PBS. Anodic sweep scan showed a peak current at 390 mV (A1) along with a shoulder at 440 mV (A2) with their corresponding counter peaks at 350 (C2) and 280 mV (C1) during the cathodic run at a scan rate of 50 mV s^{-1}. The calculated formal redox potential, $E^{o'} = (E_{pa} + E_{pc})/2$ (and the peak-to-peak separation, $\Delta Ep = E_{pa} - E_{pc}$) values were 335 (1 1 0) and 380 (90) mV respectively for the A1/C1 and A2/C2 redox processes, which could be attributed to Na^+ coupled electrochemical reaction between the Fe(III) and Fe(II) in two different forms of the complex, as proposed for the conventional bulk electrode in 1 M KNO_3 [4], as follows:

$$\{Ni^{II}_{1.5}[Fe^{III}(CN)_6] - f - MWCNT\} + Na^+ + e^- \Longleftrightarrow \{NaNi^{II}_{1.5}[Fe^{II}(CN)_6] - f - MWCNT\}(A1/C1) \quad (1)$$

$$\{NaNi^{II}[Fe^{III}(CN)_6] - f - MWCNT\} + Na^+ + e^- \Longleftrightarrow \{Na_2Ni^{II}[Fe^{II}(CN)_6] - f - MWCNT\}(A2/C2) \quad (2)$$

Note that the $E^{o'}$ values for the Ni-NCFe in f-MWCNT matrix (335 and 380 mV vs. Ag/AgCl) were different compared to the conventional bulk electrode (490 and 600 mV vs. Ag/AgCl) [4], mostly accountable as due to the difference in cation (K^+ ion in Ref. [4] vs. Na^+ ion in the present study) (see Fig. 8B), in addition to the synergic effect of the individual components within the matrix (*vide infra*). Effect of scan rates yielded systematic increase in the peak

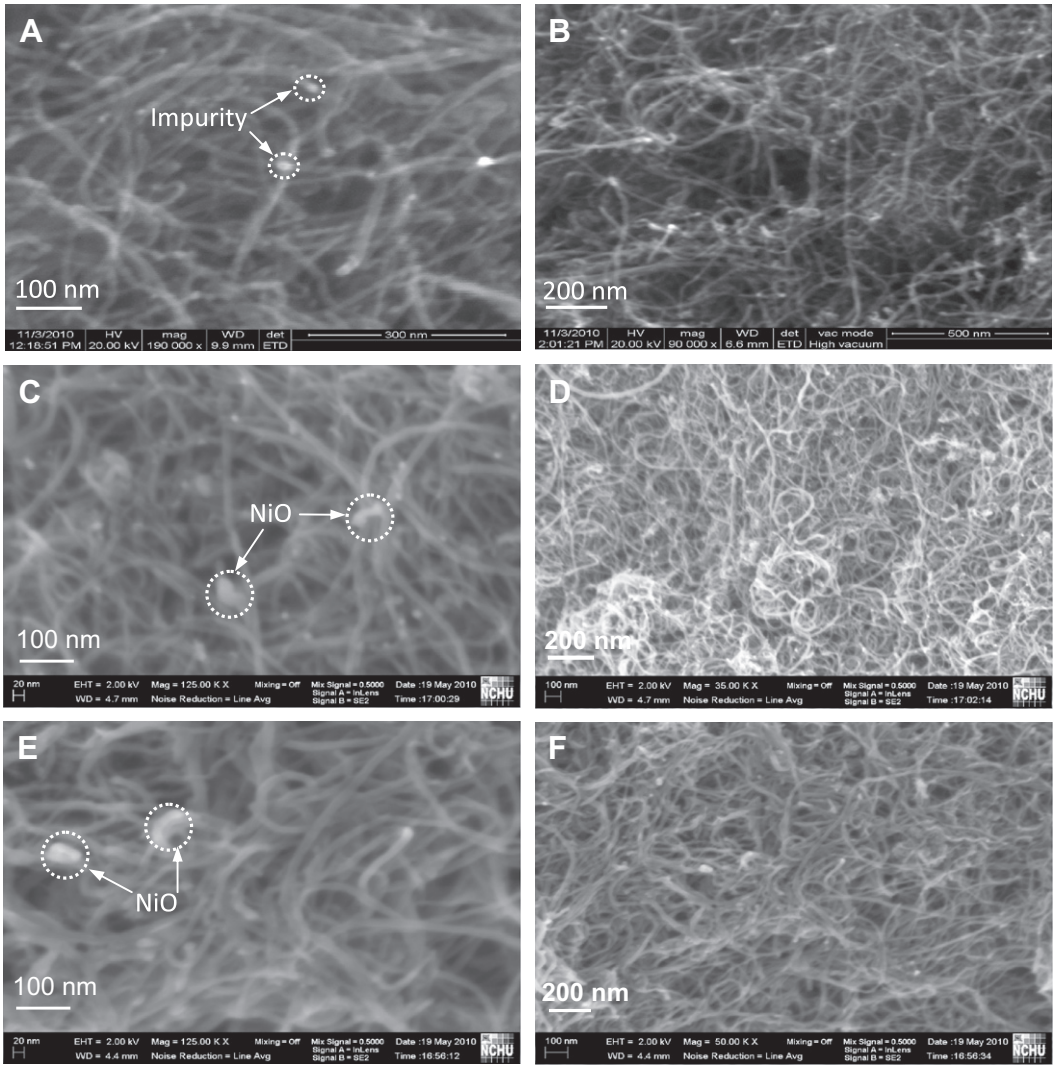

Fig. 3. FESEM images of f-MWNT (A and B), Ni@f-MWCNT (C and D) and Ni-NCFe@f-MWCNT (E and F) modified screen-printed carbon electrodes at different magnifications.

currents (i_p) upon increasing the scan rates (Fig. 6A), and the double logarithmic plots of i_{pa} and i_{pc} vs. scan rate (v) resulted in slope values ($\partial \log (i_p)/\partial \log (v)$) around 0.80 (Fig. 6B). This value is in between that expected for a completely diffusion-controlled electron-transfer process (0.5) and a surface-confined adsorption-controlled electron-transfer process (1.0), indicating that both anodic and cathodic electron transfer reactions within the hybrid matrix are under the control of both diffusion (K^+ ion diffusion in and out of the film) as well as surface adsorption. Contrast to this behavior, the bulk Ni-NCFe modified electrode has been reported [9] to follow a purely surface-confined redox process at slow sweep rates up to 300 mV s^{-1} and switch-over to diffusion-controlled mechanism at higher sweep rates. Evidently, the combined adsorption and diffusion-controlled mechanism observed in this work for the Ni-NCFe@f-MWCNT material, right from the lowest scan rate, can be taken as an evidence for the presence of both easily-accessible Ni-NCFe surface sites on the outer sides of f-MWNT with adsorption-controlled behavior, and difficultly-accessible Ni-NCFe active sites on the inner walls of f-MWNT with the charge transfer step coupled to a restricted Na^+ ion diffusion through hydrophobic basal planes of f-MWNT (rds). Continuous CV cycles of the film in pH 7 PBS showed virtually unaltered behavior with a relative standard deviation (RSD) value 1.46% (Fig. 5A), clearly showing that the introduction of Ni-NCFe within the f-MWCNT did not affect the electron-transfer process of the hybrid-f-MWCNT material in the physiological pH. The surface excess of the Ni-NCFe, $\Gamma_{\text{Ni-NCFe}}$ was calculated to be 28.8 nmol cm^{-2} within the matrix.

Several control experiments were carried out with an aim to quantitatively understand the mechanism and influencing components towards the hybrid Ni-NCFe@f-MWCNT formation. We propose a "model analyzing system" for segregation of the individual component effects, such as E1-E5, involved in the Total effect (E_T) as in the following Scheme 2. The contributing effects considered were the underlying support effect (E1), surface functional group-Ni^{2+} complexation group effect (E2), MWCNT basal plane effect (E3), impurity effect (E4), and the insertion-edge plane effect (E5).

Different types of Ni-NCFe were prepared and the respective $\Gamma_{\text{Ni-NCFe}}$ value was taken as a sensitive quantitative parameter to decouple the individual effects as in Scheme 2. First, the underlying support effect, E1, was evaluated using Ni-NCFe coated GCE (Ni^{2+} deposition at −0.9 V vs. Ag/AgCl/180 s followed by 10 min immersion in $[Fe(CN)_6]^{3-}$) as in Fig. 5B and $\Gamma_{\text{Ni-NCFe}}$ was 0.55 nmol cm^{-2}, suggesting ~5 monolayer thick Ni-NCFe film formation on the bare support. The calculated RSD value was 9.19%. For assessing the surface functional group-Ni^{2+} complexation group effect (E2), the Ni-NCFe was formed on the f-MWCNT by successively immersing the GCE/f-MWCNT in 3 mM $NiCl_2$/pH 7 PBS for 10 min, and then in

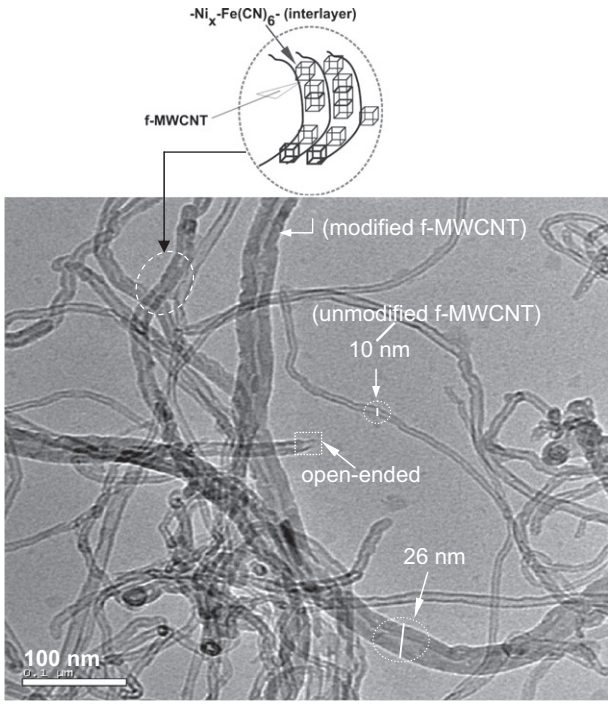

Fig. 4. TEM image of Ni-NCFe@f-MWCNT on ITO electrode.

1 mM $[Fe(CN)_6]^{3-}$ containing 0.1 M pH 7 PBS solution for 10 min at *open-circuit* condition. It was expected that the Ni^{2+} and its related species would get complexed with the available oxygen containing surface function groups as in Scheme 2 (E2). The CV of the as prepared hybrid E2 electrode material was given in Fig. 5C with a $\Gamma_{Ni\text{-}NCFe}$ and RSD of 1.26 nmol cm^{-2} and 11.4%, respectively. Meanwhile, additional control experiments such as conditioning the Ni-f-MWMT in 0.1 M NaOH (insert Fig. 5D) or 1 V anodic deposition of Ni^{2+} on GCE/f-MWCNT, followed by immersion in $[Fe(CN)_6]^{3-}$ solution were tried, to understand the role of Ni oxide/hydroxide ($NiO/Ni(OH)_2$) in the Ni-NCFe formation. Note that such pretreatment procedures failed to show any Ni-NCFe@f-MWCNT formation (Fig. 5D&E), conclusively proving that NiO and $Ni(OH)_2$ species were not involved in the hybrid material formation in this work. As a next step, the effect of MWCNT basal plane, E3, was probed by studying GCE/untreated MWCNT (as received) (E3) and GCE/purified MWCNTs (E3') with Ni-NCFe deposited on them electrochemically (Ni^{2+} electrodeposition and subsequent immersion in $[Fe(CN)_6]^{3-}$ solution). Fig. 7A and B are typical CV responses of 'as received' and 'purified' MWCNTs with $\Gamma_{Ni\text{-}NCFe}$ values of 6.15 and 5.84 nmol cm^{-2}, respectively. These values were ~5 times lower than the response of GCE/Ni-NCFe@f-MWCNT (i.e., E_T, 28.8 nmol cm^{-2}), indicating that the basal planes could contribute only marginally (22%) to the hybrid material formation. The difference in the $\Gamma_{Ni\text{-}NCFe}$ values for 'as received MWCNT' (E3) and 'purified MWCNT' (E3') could be taken as a measure for the impurity effect, E4. The calculated difference was 0.31 nmol cm^{-2}. Some of the major impurities within the MWCNT are iron and amorphous carbon [34], which were found to contribute 1% (E4 effect) to the total (E_T, 28.8 nmol cm^{-2}). The final component i.e., insertion-edge plane effect (E5), could be calculated by deducting the contributions E1 + E2 + E3 + E4 from E_T, and the value of E5 = 20.53 nmol cm^{-2}, which is equal to 71.3% in the overall effect, E_T. This observation particularly stresses that the insertion of the Ni^{2+} within the edge plane defect holes, during the cathodic electrochemical deposition at −0.9 V potential step, held the major share for the enhanced loading of the Ni-NCFe units within the f-MWCNT. Fig. 7C shows the% contribution of the individual components. This mechanistic model provides an excellent support for the presence of edge-plane hole defects and oxygen functionalities, recently reported by Compton group for the carbon nanotubes [36].

The effect of solution pH and alkali metal ion concentration was studied with the GCE/Ni-NCFe@f-MWCNT material (Figs. 6C and 8). A change in the solution pH, in the range 3–10 (Fig. 6C), on the CV response of the GCE/Ni-NCFe@f-MWCNT showed virtually unaltered E_{pa} suggesting the absence of any proton accessible sites within the hybrid matrix. Similarly, low ionic radii alkali metals, Li^+ and Na^+ (Fig. 8A) also showed unaltered i_p and E_{pa} upon changing their concentration in the window of 0.01 M-0.15 M, due to the feasible and reversible electron-transfer coupled Na^+ insertion reaction in agreement with classical Ni-NCFe system [4,22,23]. Ions with higher ionic radii viz., K^+, NH_4^+ and Ba^{2+} resulted in marked shift in the redox potential of the Ni-NCFe@f-MWCNT to higher values (Fig. 8B), which is also in parallel with the bulk Ni-NCFe material [22], strongly suggesting that the Ni-NCFe within the f-MWCNT retains the macro-molecular zeolite structure with cavity diameter 1.8 Å [22], with the result the alkali metal ions with diameter above this size have difficulty to access the active sites leading to alteration in the electrochemical parameter.

The effect of KCl concentration on the GCE/Ni-NCFe@f-MWCNT's redox response is given in Fig. 8C. Changes in the E_{pa} and E_{pc} values were systematic. Fig. 8D shows the typical plot of peak potentials against log[KCl] measured from the CV traces. The slope (∂E_{pa} or $\partial E_{pc}/\partial$log [KCl]) values obtained were non-Nernstian: 42.9 and 117 mV/decade, different from the Nernstian value (60 mV/decade), suggesting that the redox reactions could occur with the participating K^+/e^- species taking part as non-integrals (with expected slope) $2\,K^+/3e^-$ (40 mV) and $2\,K^+/e^-$ (120 mV) respectively, for the anodic and cathodic processes. Such an observation was never reported in the literature for the bulk Ni-NCFe. However, hydrous ruthenium oxides were reported to follow such a non-Nernstian behavior against the solution pH ($\partial E_{pa}/\partial$pH ~ −75 mV/decade), due to the presence of accessible and non-accessible surface sites [47–49]. The behavior of K^+ with Ni-NCFe@f-MWCNT can be understood since the nanocubic Ni-NCFe units within the f-MWCNT could access (insertion) the K^+ ions relatively slowly during the cathodic process than the faster exertion of K^+ in the anodic side. Presumably, major part of the insertion and exertion are through the basal planes of f-MWCNT, and since these are hydrophobic in character, there could be some kinetic limitation for the K^+ to get into the inner walls through the basal plane (Scheme 3). On the other hand, the easy exertion process might be due to the presence of the internal water-channels [45,46], into which the K^+ ions could be transferred rapidly at relatively faster rates in the anodic side. Note that no such complication could be observed for the Na^+ within the Ni-NCFe@f-MWCNT, since apart from its low ionic radii, its presence at 0.61 atomic% in the internal matrix (Table S1) is a key to stabilize the Ni-NCFe@f-MWCNT in sodium containing pH 7 PBS.

3.3. Electrocatalytic and amperometric sensing behaviors

Hydrazine electrocatalytic behavior on the GCE/Ni-NCFe@f-MWCNT at pH 7 PBS is demonstrated in Fig. 9A. As can be seen from the CV curves, the unmodified GCE/f-MWCNT showed the starting oxidation potential for hydrazine at 0.15 V with feeble oxidation current signal (curve c) on the anodic side, while the GCE/Ni-NCFe@f-MWCNT showed the oxidation current response starting from 0.05 V and maximizing at 0.390 V vs. Ag/AgCl, the potential coinciding with that of $Ni\text{-}NCFe^{II}$ to $Ni\text{-}NCFe^{III}$ transformation in the Ni-NCFe@f-MWCNT material (Fig. 5A). A substantial increase in the catalytic current, ca. 33 times and a 100 mV reduction in the

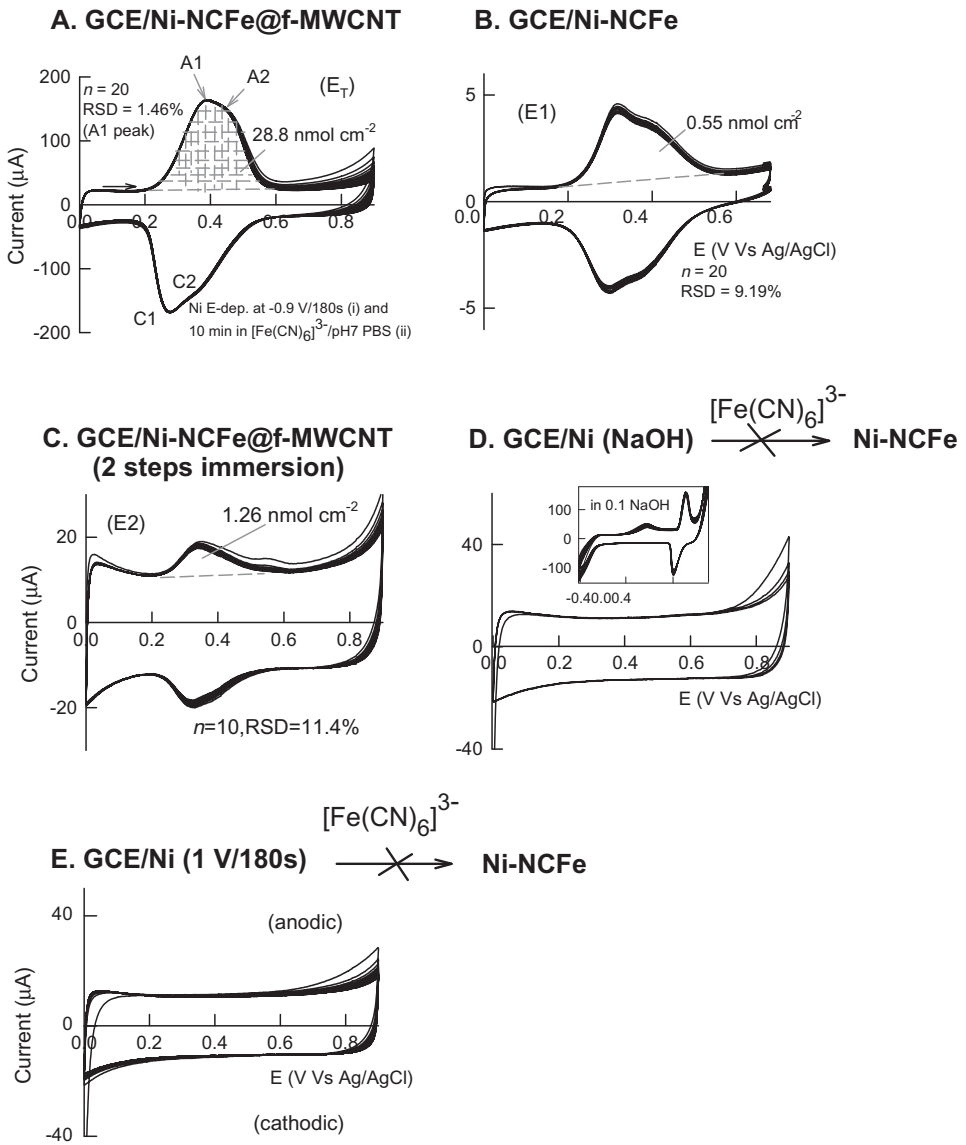

Fig. 5. CV responses of various f-MWCNT modified electrodes (A–E) in pH 7 sodium phosphate buffer solution at a scan rate of 50 mV s^{-1}. Figure D is response of GCE/Ni@f-MWCNT treated in 0.1 M NaOH solution (insert) followed by immersion in 1 mM $[Fe(CN)_6]^{3-}$/10 min. Figure E is response of GCE/Ni@f-MWCNT prepared by anodic Ni deposition (3 mM Ni^{2+}, 1 V vs. Ag/AgCl for 180 s) followed by immersion in 1 mM $[Fe(CN)_6]^{3-}$ /10 min.

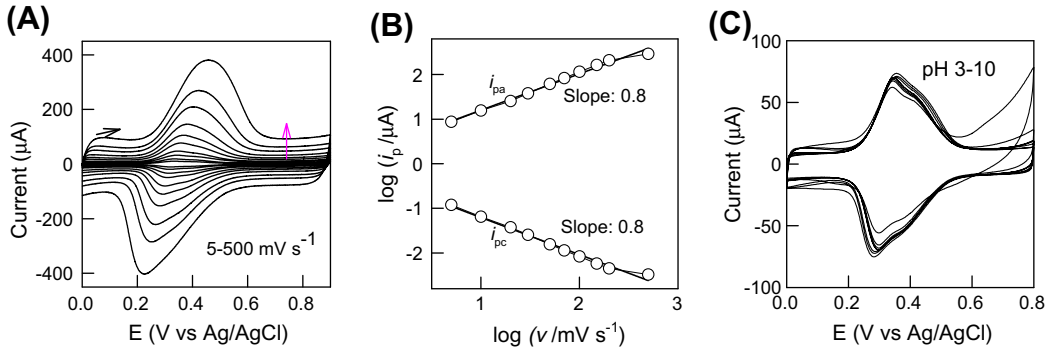

Fig. 6. Effect of CV scan rate on GCE/Ni-NCFe@f-MWCNT in pH 7 PBS (A); plot of double logarithmic of peak currents vs. scan rate (B); effect of solution pH on CV responses of GCE/Ni-NCFe@f-MWCNT at v = 50 mV s^{-1} (C).

over-potential could be noticed with this new hybrid material demonstrating the enhanced electrocatalytic feature of the material in pH 7 PBS. Extended hydrazine oxidation experiments with other control electrodes, as listed in Fig. 5B and C and Fig. 7A–B, resulted in about 10–30 times lowered catalytic currents than the response current shown by GCE/Ni-NCFe@f-MWCNT, confirming

E_T = $E1_{support}$ + $E2_{complexation}$ (surf.funct. group/binding) + $E3_{basal\ plane}$ + $E4_{impurites}$ + $E5_{inserstion\text{-}edge\ plane}$ (?)

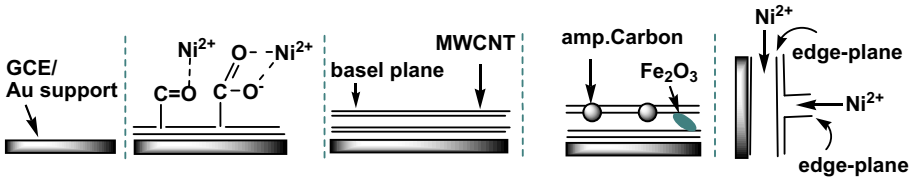

Scheme 2. Possible influencing components towards the hybrid Ni@f-MWCNT and in Turn Ni-NCFe@f-MWCNT formation. E5 = E_T – (E1 + E2 + E3 + E4). amp = amorphous.

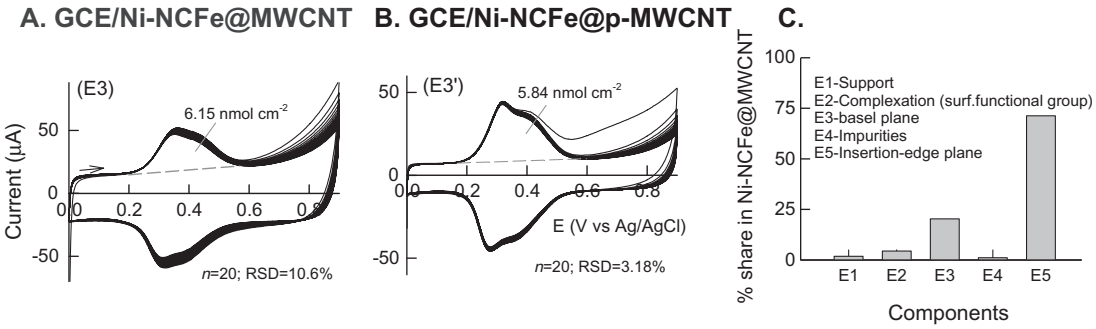

Fig. 7. CV responses of GCE/Ni-NCFe@MWCNT (MWCNT as received) (A), GCE/Ni-NCFe@p-MWCNT (p = purified) (B) in pH 7 PBS at $v = 50$ mV s^{-1}. (C) Typical plot for the% share on Ni-NCFe@f-MWCNT formation vs. contributing components.

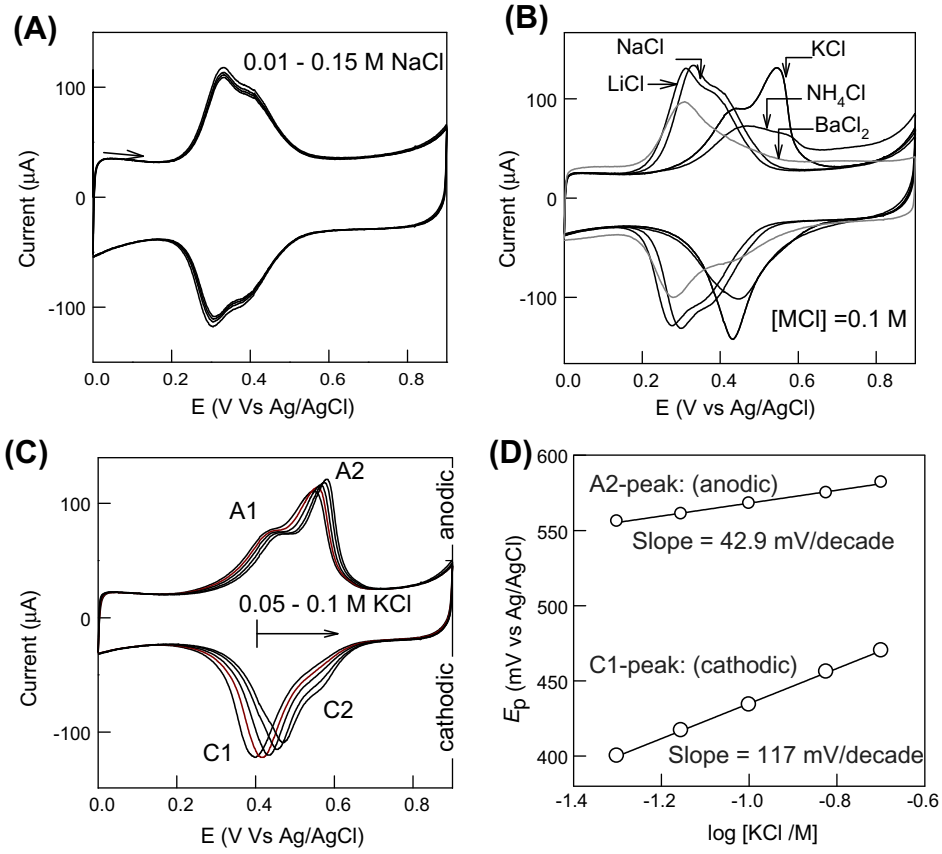

Fig. 8. CV responses of GCE/Ni-NCFe@f-MWCNT in different aqueous solutions: (A) 0.01–0.15 M NaCl; (B) 0.1 M of LiCl, NaCl, KCl, NH_4Cl and $BaCl_2$; (C) 0.05–0.1 M KCl ($v = 50$ mV s^{-1}). (D) Typical plot of peak potential vs. log[KCl].

the superior and enhanced catalytic behavior of the GCE/Ni-NCFe@f-MWCNT system. Continuous CV cyclings ($n = 20$) of the hydrazine on the GCE/Ni-NCFe@f-MWCNT electrode did not show any marked alteration in the current signals and this observation clearly indicated that the hydrazine oxidized products, $4H^+$ and N_2, did not influence the stability of the matrix. The anodic peak

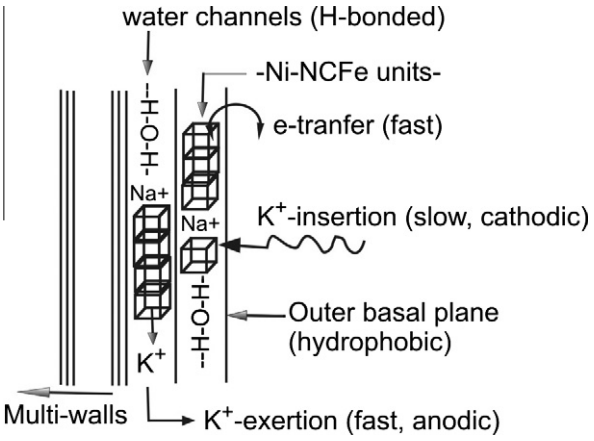

Scheme 3. Cartoon for the K^+ insertion and exertion reactions within the Ni-NCFe@f-MWCNT.

current, i_{pa}, showed a linear relationship between $\log(i_{pa})$ against $\log(v)$ with a slope of 0.6 (inset Fig. 9A(a)), indicating that the catalytic oxidation reaction of hydrazine at the GCE/Ni-NCFe@f-MWCNT electrode is (substrate) diffusion-controlled [50], which attests to a rapid (not rate controlling) reaction between Fe^{III} in the film and hydrazine in solution. The electrocatalytic oxidation of hydrazine followed the typical EC_{CAT} mechanism involving Ni-$NCFe^{II}$ to Ni-$NCFe^{III}$ electron transfer reaction with a succeeding cross-exchange reaction between the hydrazine and the electro-generated Ni-$NCFe^{III}$ active sites, similar to the classical system, for instance Ni-NCFe entrapped sol–gel matrix for hydrazine oxidation at pH 7 PBS + 0.5 M NaCl system [9]. However, compared to the previous system, the catalytic peak current from CV measurements was found to be linear with the concentration of hydrazine up to 3 mM (Fig. 9A(b) inset) with current sensitivity of 19.7 μA/mM, which is about 20 times sensitive over the sol–gel modified Ni-NCFe (~1 μA/mM) [9]. Such an enhanced catalytic activity for the GCE/Ni-NCFe@f-MWCNT electrode could originate from a combination of an increased availability of inner-walls-bound Ni-NCFe sites within the f-MWCNT and macro-molecular Ni-NCFe units precipitated on the CNT surface that is clearly distinct from the traditional *ex-situ* preparation approach [11,12,26–29], where the catalyst particles were assembled/adsorbed exclusively on the external surface of the CNT. Extended amperometric detection methods as in Fig. 9B and C, yielded linear calibration plot in the window of 20–200 μM of hydrazine with a sensitivity of 120.2 μA/μM (R = 0.998) for the GCE/Ni-NCFe@f-MWCNT electrode. The calculated detection limit (S/N = 3) was 620 nM. The hybrid electrode showed tolerance to interference chemicals such as citric acid, oxalic acid and nitrite, all of which are of industrial and pharmacological interest, and often reported to compete with the hydrazine detection [51]. In some cases, Nafion was used as an over layer coating to enhance the stability and to eliminate the interferences [51]. But no such specific extraneous treatment is required in this present case, which again confirms the promising electro-analytical performance of the present hybrid material. Finally, real sample assays for the detection of hydrazine present in three different kinds of water samples could

Table 2
Results of the hydrazine real sample analysis obtained using a GCE/Ni-NCFe@f-MWCNT by amperometric *i–t* method at an applied potential of 350 mV vs. Ag/AgCl in pH 7 PBS.

Real sample	Hydrazine concentration (μM)			Recovery%
	Original detected	Spiked	Detected after spike	
1. Drinking water	0	20	20.29	98.57
		40	38.14	104.80
		60	62.17	96.70
		80	79.22	100.98
2. Well water	0	20	19.85	100.78
		40	41.80	95.69
		60	60.34	99.45
		80	78.85	101.46
3. Bore water	0	20	20.03	99.80
		40	38.04	105.10
		60	58.65	102.20
		80	82.10	97.50

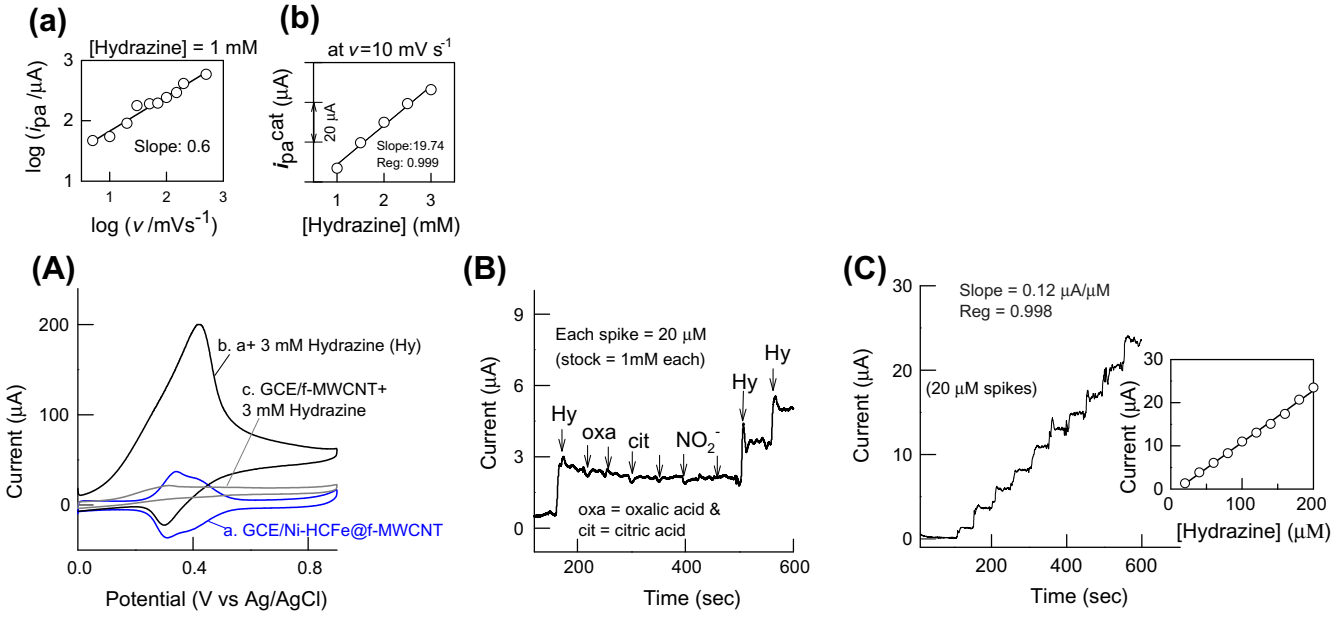

Fig. 9. (A) CV of GCE/Ni-NCFe@f-MWCNT without (a) and with 3 mM of hydrazine (b), and GCE/f-MWCNT with 3 M hydrazine (c) in pH 7 PBS at $v = 50$ mV s^{-1}. (B) and (C) are typical amperometric response of GCE/Ni-NCFe@f-MWCNT for detection of hydrazine with interference chemicals and continuous spiking of hydrazine, respectively, at an applied potential of 350 mV vs. Ag/AgCl in pH 7 PBS. Insert figures in (A) and (C) are double log i_{pa} vs. scan rate and calibration plots.

be successfully demonstrated with recovery values in the range 95.69–105.10% (Table 2), which further validate the usefulness of the GCE/Ni-NCFe@f-MWCNT working electrode for practical analysis.

4. Conclusions

A hybrid nickel-hexacyanoferrate-multiwalled carbon nanotube chemically modified glassy carbon electrode (GCE/Ni-NCFe@f-MWCNT) has been prepared by a new *in situ* precipitation technique using electrochemically deposited GCE/Ni@f-MWCNT as a template and $[Fe(CN)_6]^{3-}$ as a precipitant, without any additional interlinking agent. The resulted hybrid GCE/Ni-NCFe@f-MWCNT showed a very high Ni-NCFe active site accumulation and excellent stability in pH 7 sodium PBS. Characterization by XRD, XPS, FESEM, EDXA and TEM indicated availability of large number of edge-plane hole defects with oxygen functionality, which are quite suitable for accumulation of vast amount of Ni^{2+} species by electrochemical deposition and subsequent *in situ* precipitation of the hybrid material. The Ni-NCFe exists as nanocubic chains within the pathways of the MWCNT. Various controlling factors in the hybrid material formation were studied, and the 'Ni^{2+} metal insertion within the edge-plane defect' step was found to contribute maximum to the total effect. The new material was similar in its electrochemical behavior to the conventional bulk Ni-NCFe that two different forms of the complex, namely, $\{Ni^{II}_{1.5}[Fe^{III}(CN)_6]@f-MWCNT\}$ and $\{NaNi^{II}[Fe^{III}(CN)_6@f-MWCNT\}$ would participate in the electrochemical reactions for both materials; however, the new material differed and showed the existence of accessible and non-accessible surface sites, revealed as non-stoichiometry values for the participating species (K^+/e^-) as $2\ K^+/3e^-$ and $2\ K^+/e^-$, for the anodic and cathodic processes, respectively, an interesting observation for the first time for the nickel-hexacyanoferrate material. Besides, the stability in pH 7 PBS, electrochemical and hydrazine electrocatalytic features of the newly developed GCE/Ni-NCFe@f-MWCNT were superior over the bulk Ni-NCFe material.

Acknowledgements

The authors gratefully acknowledge financial support from Department of Science and Technology, India. We also thank Prof. Jyh-Myng Zen for his valuable discussions on this manuscript.

Appendix A. Supplementary material

Figure S1 for CV response of simulated Ni-NCFe@f-MWNT powder modified GCE and Figure S2 and Table S1 for EDXA results of Ni@f-MWCNT and Ni-NCFe@f-MWCNT samples. Supplementary data associated with this article can be found, in the online version, at doi:10.1016/j.jelechem.2011.01.022.

References

[1] T. Takenobu, T. Takano, M. Shiraishi, Y. Murakami, H. Kataura, Y. Achiba, et al., Nature Mater. 2 (2003) 683.
[2] A.S. Kumar, P. Swetha, Langmuir 26 (2010) 6874.
[3] A.S. Kumar, S. Sornambikai, L. Deepika, J.-M. Zen, J. Mater. Chem. 20 (2010) 10152.
[4] W. A Steen, S.W. Han, Q. Yu, R.A. Gordon, J.O. Cross, E.A. Stern, et al., Langmuir 18 (2002) 7714.
[5] K. Itaya, N. Shoji, I. Uchida, J. Am. Chem. Soc. 106 (1984) 3423.
[6] P. M. S. Monk, R. J Mortimer and D. R Rosseinsky, Electrochromism: Fundametals and Applications, Ch. 6, VCH, Weinheim (1995).
[7] H. Xiaogang, T.S. Daniel, Chem. Mater. 17 (2005) 5831.
[8] K.M. Jeerage, W.A. Steen, D.T. Schwartz, Chem. Mater. 14 (2002) 530.
[9] A. Salimi, K. Abdi, Talanta 63 (2004) 475.
[10] A. Abbaspour, A. Khajehzadeh, A. Ghaffarinejad, J. Electroanal. Chem. 631 (2009) 52.
[11] M. Yang, Y. Yang, F. Qu, Y. Lu, G. Shen, R. Yu, Anal. Chim. Acta 571 (2006) 211.
[12] X. Cui, G. Liu, Y. Lin, J. Biomed. Nanotechnol. 1 (2005) 320.
[13] S.J.R. Prabakar, S.S. Narayanan, Electroanalysis 21 (2009) 1481.
[14] D.M. Zhou, H.X. Ju, H.Y. Chen, J. Electroanal. Chem. 408 (1996) 219.
[15] A.V. Krylov, F. Lisdat, Electroanalysis 19 (2007) 23.
[16] H.B.F.Y. Yon, C.R. Lowe, Anal. Chem. 59 (1987) 2111.
[17] C.X. Cai, H.X. Ju, H.Y. Chen, Anal. Chim. Acta 310 (1995) 145.
[18] C. Cai, H. Ju, H. Chen, Anal. Lett. 28 (1995) 820.
[19] U. Scharf, E.R. Grabner, Electrochim. Acta 41 (1996) 233.
[20] J. Bácskai, K. Martinusz, E. Czirók, G. Inzelt, P.J. Kulesza, M.A. Malik, J. Electroanal. Chem. 385 (1995) 241.
[21] A.B. Bocarsly, S. Sinha, J. Electroanal. Chem. 137 (1982) 157.
[22] S. Sinha, B.D. Humphrey, A.B. Bocarsly, Inorg. Chem. 23 (1984) 203.
[23] S. Bharathi, V. Yegnaraman, G.P. Rao, Langmuir 11 (1995) 666.
[24] J.A. Lopez, J. Manríquez, S. Mendoza, L.A. Godínez, Electrochem. Commun. 9 (2007) 2133.
[25] N. Bagkar, S. Choudhury, S. Bhattacharaya, J.V. Yakhmi, J. Phys. Chem. B 112 (2008) 6467.
[26] Y. Lin, X. Cui, J. Mater. Chem. 16 (2006) 585.
[27] L. Qian, X. Yang, Talanta 69 (2006) 957.
[28] S. Wang, L. Lu, M. Yang, Y. Lei, G. Shen, R. Yu, Anal. Chim. Acta 651 (2009) 220.
[29] B. Fang, Y. Wei, M. Li, G. Wang, W. Zhang, Talanta 72 (2007) 1302.
[30] H.O. Sjogren, Cancer 45 (1980) 1229.
[31] L. Carlsen, B.N. Kenessov, S.Y. Batyrbekova, S.Zh. Kolumbaeva, T.M. Shalakhmetova, Environ. Toxicol. Pharmacol. 28 (2009) 448.
[32] P.D. Tam, J. Immunol. Methods 350 (2009) 118.
[33] E.B. Craig, C. Alison, S. Christopher, J.W. Shelley, R.G. Compton, Angew. Chem. Int. Ed. 45 (2006) 2533.
[34] CRC handbook of chemistry and physics, R.C Weast and D.R Lide [Eds.], CRC press, Florida, 1989.
[35] K.J. Hae, P.L. Yun, H.J. Mei, S.K. Eun, J.B. Jung, H.L. Young, Chem. Phys. Lett. 470 (2009) 255.
[36] A.F. Holloway, G.G. Wildgoose, R.G. Compton, L. Shao, M.L.H. Green, J. Solid State Electrochem. 12 (2008) 1337.
[37] P. Azadi, R. Farnood, E. Meier, J. Phys. Chem. A 114 (2010) 3962.
[38] S.J. Park, G.H. Shim, H.Y. Kim, J. Colloid Interf. Sci. 291 (2005) 585.
[39] M. Chigane, M. Ishikawa, J. Chem. Soc. Faraday Trans. 94 (1998) 3665.
[40] A.P. Grosvenor, M.C. Biesinger, R.StC. Smart, N.S. McIntyre, Surf. Sci. 600 (2006) 1771.
[41] P. Druska, H.H. Strehblow, Surf. Interfact. Anal. 23 (1995) 440.
[42] X. Tan, M. Fang, C. Chen, S. Yu, X. Wang, Carbon 46 (2008) 1741.
[43] G.E. Benedetto, M.R. Guascito, R. Ciriello, R.I. Cataldi, Anal. Chim. Acta 410 (2000) 143.
[44] T.R.I. Cataldi, R. Guascito, A.M. Salvi, J. Electroanal. Chem. 417 (1996) 83.
[45] H.N. William, D.A. Kevin, E.S. Richard, M. Jianpeng, Chem. Phys. Lett. 355 (2002) 445.
[46] M. Yutaka, K. Hiromichi, A. Masatoshi, U. Akiko, S. Shinzo, A. Yohji, et al., Chem. Phys. Lett. 401 (2005) 534.
[47] A.S. Kumar, K. Chandrasekara Pillai, J. Solid State Electrochem. 4 (2000) 408.
[48] V. Dharuman, K. Chandrasekara Pillai, J. Solid State Electrochem. 10 (2006) 967.
[49] M.E.G. Lyons, L.D. Burke, J. Chem. Soc. Faraday Trans I 83 (1987) 299.
[50] F. Scholtz, Electroanalytical Methods: Guide to Experiments and Applications, Springer, Berlin, Heidelberg, 2002.
[51] J.M. Zen, A.S. Kumar, Acc. Chem. Res. 34 (2001) 772.